Author(s): Broas, Mikael; Jiang, Hua; Graff, Andreas; Sajavaara, Timo; Vuorinen, Vesa; Paulasto-Kröckel, Mervi

Title: Blistering mechanisms of atomic-layer-deposited AlN and Al2O3 films

Year: 2017

Version:

Please cite the original version:

Broas, M., Jiang, H., Graff, A., Sajavaara, T., Vuorinen, V., & Paulasto-Kröckel, M. (2017). Blistering mechanisms of atomic-layer-deposited AlN and Al2O3 films. Applied Physics Letters, 111(14), Article 141606. https://doi.org/10.1063/1.4994974

Blistering mechanisms of atomic-layer-deposited AlN and Al_2O_3 films

Mikael Broas, Hua Jiang, Andreas Graff, Timo Sajavaara, Vesa Vuorinen, and Mervi Paulasto-Kröckel

Citation: Appl. Phys. Lett. **111**, 141606 (2017); doi: 10.1063/1.4994974
View online: http://dx.doi.org/10.1063/1.4994974
View Table of Contents: http://aip.scitation.org/toc/apl/111/14
Published by the American Institute of Physics

Blistering mechanisms of atomic-layer-deposited AlN and Al_2O_3 films

Mikael Broas,[1,a)] Hua Jiang,[2] Andreas Graff,[3] Timo Sajavaara,[4] Vesa Vuorinen,[1] and Mervi Paulasto-Kröckel[1]

[1]*Aalto University, Department of Electrical Engineering and Automation, P.O. Box 13500, FIN-00076 Aalto, Espoo, Finland*
[2]*Aalto University, Nanomicroscopy Center, P.O. Box 15100, FIN-00076 Aalto, Espoo, Finland*
[3]*Fraunhofer Institute for Microstructure of Materials and Systems IMWS, Walter-Huelse-Str. 1, 06120 Halle, Germany*
[4]*University of Jyvaskyla, Department of Physics, P.O. Box 35, FIN-40014, Jyvaskyla, Finland*

(Received 9 July 2017; accepted 13 September 2017; published online 4 October 2017)

Blistering of protective, structural, and functional coatings is a reliability risk pestering films ranging from elemental to ceramic ones. The driving force behind blistering comes from either excess hydrogen at the film-substrate interface or stress-driven buckling. Contrary to the stress-driven mechanism, the hydrogen-initiated one is poorly understood. Recently, it was shown that in the bulk Al-Al_2O_3 system, the blistering is preceded by the formation of nano-sized cavities on the substrate. The stress- and hydrogen-driven mechanisms in atomic-layer-deposited (ALD) films are explored here. We clarify issues in the hydrogen-related mechanism via high-resolution microscopy and show that at least two distinct mechanisms can cause blistering in ALD films. *Published by AIP Publishing.* [http://dx.doi.org/10.1063/1.4994974]

Blistering in films grown by atomic layer deposition (ALD) takes place for various substrate-film combinations[1–3] and is typically observed after high-temperature treatments.[4] Blisters are generally treated as reliability risks as they create mechanically weak spots in protective and structural coatings[5] but can be also exploited in rear semiconductor-metal contact formation of passivated solar cells.[6] Most studies regarding blistering of ALD films deal with Al_2O_3 as it is one of the most thoroughly characterized ALD material and since it provides excellent passivation of Si-based solar cells.[6–9] The passivated solar cells undergo a firing step to improve the interfacial quality between the Al_2O_3 film and the Si substrate, after which the semispherical defects appear on the film. The blistering is thought to be caused by desorbing H_2 and H_2O vapor that gets trapped between the substrate and the film.[9] The ALD film acts as a gas diffusion barrier, while the interfacial gas pressure grows finally causing local delamination and bulging of the film. However, recently Xie *et al.* [10] showed that in order to initiate the delamination and the blister formation from a nm-order defect site, an unrealistically high gas pressure of tens of gigapascals would be required. Therefore, a subcritical defect (subcritical gas bubble) has to grow first before the macroscopic delamination and blister formation can occur. They showed that in the bulk Al-Al_2O_3 system, the initiation of blister formation is indeed driven by trapped hydrogen at the interface, but before the macroscopic delamination occurs, cavitation of the substrate takes place creating suitable nucleation sites for the blisters. Furthermore, they postulated that the cavitation is caused by surface diffusion of the substrate, which occurs after the hydrogen at the interface has undermined the bonds between the film and substrate, therefore effectively creating a free surface that can reconstruct according to its Wulff construction.

However, on the contrary to the *in-situ* environmental transmission electron microscopy (TEM) study of Xie *et al.*,[10] the ALD studies have only presented evidence of the macroscopic blisters, which includes optical,[1–3,6–8,11] atomic force microscopy,[2,11] scanning electron microscopy,[2,6,7] and cross-sectional focused ion beam[2,8] images. Since ALD is typically realized on Si substrates, the explanation of surface self-diffusion of the substrate may not be feasible as metallic and semiconductor substrates may not be comparable in behavior. Furthermore, the detailed structure of the blister region remains unknown as the environmental TEM images were taken from thick samples without high-resolution information. It is the scope of this communication to explore the blistering in two ALD materials—Al_2O_3 deposited by thermal ALD and AlN deposited by plasma-enhanced ALD (PEALD). The films were characterized by aberration-corrected TEM, x-ray diffraction (XRD), and time-of-flight elastic recoil detection analysis (ToF-ERDA) to investigate the blister formation mechanisms and the structure of the blisters and to compare them to the stress-states of the films and the films' chemical compositions including the hydrogen content.

The Al_2O_3 films were deposited on 150 mm (100) Si wafers with native oxide in a thermal ALD batch reactor (Beneq P400A) using trimethylaluminum (TMA) and H_2O as the precursors at 450 °C. A purge cycle was applied between the precursor half reactions. Further details can be found in Ref. 12. The AlN films were deposited on (100) Si wafers with native oxide in a PEALD reactor (Picosun R-200) with a remote inductively coupled plasma (ICP) configuration. $AlCl_3$ and NH_3/Ar plasma were used as the precursors at 500 °C with a purge cycle between the half reactions. The plasma head was operated at 2000 W. A similar setup with TMA was used in Ref. 13.

The films were characterized with an ellipsometer (Plasmos SD2300) for thicknesses and refractive indices at the wavelength of 632.8 nm. The Al_2O_3 films were annealed

a)Author to whom correspondence should be addressed: mikael.broas@aalto.fi

at 1000 °C in high vacuum (HV) conditions ($p_{tot} < 10^{-6}$ mbar) in a furnace (Webb Red Devil M) (the HV annealing experiment was repeated three times to confirm the results). The annealing time at the peak temperature was 1 h, and the ramp rate up was 10 °C/min, whereas cooling was achieved with natural heat dissipation. The electron transparent cross-sectional lamellas were prepared with focused ion beam systems (FEI, Zeiss, and Tescan). Final polishing was done at 5 kV. The AlN film was imaged with an image C_s-corrected microscope at 300 kV (FEI Titan^3 G2 60-300) equipped with a silicon drift detector (Super-X) energy dispersive x-ray spectrometer (EDX). The Al_2O_3 film was imaged with an image and probe double C_s-corrected microscope at 200 kV (JEOL JEM-2200FS) equipped with an EDX. Symmetrical θ-2θ XRD analysis was carried out with an x-ray diffractometer (Rigaku SmartLab) equipped with a 9 kW rotating Cu anode source. The incident beam was monochromatized using a multilayer mirror and a Ge (220) double bounce monochromator. Finally, chemical analyses were done using ToF-ERDA with 11.9 MeV $^{63}Cu^{7+}$ ions.[14]

The thickness/growth per cycle/refractive index/non-uniformity of the Al_2O_3 films was 100 nm/0.07 nm/1.66/1%. The alumina films were previously characterized in Ref. 12 and represent typical high-temperature ALD alumina. It needs to be noted that the TMA precursor starts to decompose at around 370 °C, which could cause chemical vapor deposition (CVD) type growth and hence lower film quality.[15,16] However, as noted later, the ToF-ERD results show the as-deposited alumina film to be of high-quality and the CVD effects are considered not to affect the film composition in an adverse manner. Furthermore, the 1000 °C temperature treatment increased the refractive index to 1.70 while the thickness decreased to approximately 95 nm. The PEALD $AlCl_3$-based AlN film's properties in the same order as above were measured to be 58 nm/0.03 nm/1.99/9%. In another study about the deposition of AlN by PEALD from $AlCl_3$ by Lee and Kang,[17] the growth per cycle at 350 °C was saturated at 0.04 nm/cycle. The different growth rates may originate from the different reactor setups. It is also possible that the growth rate was hindered due to the underdosing of the reactants. However, the $AlCl_3$ dosing was optimized through thermal ALD process development where 0.08 nm/cycle was achieved. A closer examination of the process development is under preparation.

Visual inspection of the AlN and the Al_2O_3 films after annealing revealed a high density of bright dots (i.e., blisters) on the surfaces of the films (see Fig. S1, supplementary material). The number of the blisters was higher in the Al_2O_3 film. It has been previously shown that it is possible to affect both the number and size of blisters by selecting appropriate growth and annealing conditions. In addition, no blisters are formed for thin layers of a few nm.[2,6,8,9,11]

Two TEM samples were prepared to inspect the films and blisters (Figs. 1 and 2). The local nanostructures of the blisters are different in the AlN and the Al_2O_3 samples. In the AlN sample, blistering occurred through buckling of the film, i.e., the film had delaminated locally while on the surface a bulge had appeared. On the contrary, in the Al_2O_3 sample, the silicon substrate had cavitated while a crack had appeared through the alumina film. In the AlN sample, the

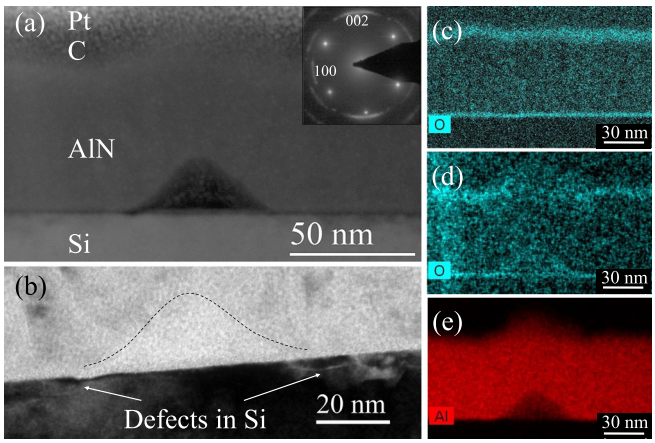

FIG. 1. TEM images of the AlN film. (a) A dark-field scanning TEM image with the selected area electron diffraction (SAED) pattern of the film and silicon in the inset. A buckle has formed in the AlN (a cavity on the Si side and a bulge on the surface). The SAED pattern is from an intact site, includes also silicon, and was taken along the Si ⟨110⟩ zone axis. The indexed, partial ring patterns show polycrystalline hexagonal AlN with slight preferential orientation with AlN [002] normal to the film interface. (b) Bright-field TEM image shows defects in Si at the edges of the AlN cavity. The dashed line is to visualize the location of the cavity. (c) EDX oxygen map at a blister-free site. (d) and (e) O and Al EDX maps at the blister site.

film surface and silicon native oxides were intact at a site without a blister [Fig. 1(c)], whereas Fig. 1(d) shows that at the blister site, both oxide layers are not fully intact and follow the buckled shape. The silicon EDX map also showed that the AlN film had not cleanly delaminated by itself (Fig. S2, supplementary material). Furthermore, the Si substrate showed defects at the edges of the wrinkle [Fig. 1(b)].

In the alumina sample, the cavitation of silicon seems to have taken place approximately following the {113} planes based on the fast Fourier transform (FFT) of Si [Fig. 2(a)]. Si {113} faceting during vacuum annealing has been also experimentally observed,[18] and the stability of {113} facets is theoretically plausible although it depends on the chemical potential of the atmosphere (e.g., hydrogen).[19] The cross-section may be towards the edge of the defect, and the lamella has a finite thickness which is why also some lattice fringes were observed where empty space would be expected. The edges of the cavity had accumulated silicon based on the high-resolution TEM and EDX inspection. Furthermore, the silicon at the edges has stacked in an epitaxial fashion. No further defects in the substrate were seen at the cavitation site. No Si diffusion into the alumina film was detected either. An image of a subcritical cavity with no crack in the alumina film can be found in Fig. S3 of the supplementary material.

These two different blistering modes were further investigated by XRD to analyze the stresses of the films and by ToF-ERDA to investigate the chemical compositions. Figure 3 presents the symmetrical θ-2θ XRD data with the peak locations extracted from the Inorganic Crystal Structure Database. The polycrystalline AlN film was oriented with the hexagonal c-axis normal to the interface, which is also visible in the SAED pattern in Fig. 1(a). The AlN indexing was according to Ref. 20. The alumina film had a more complex diffractogram and was best indexed with κ,[21] θ,[22] and α[23] phases in contrast to N_2 annealing in Ref. 12 where bare θ indexing provided the best fit. Based on the XRD data, the AlN film is in

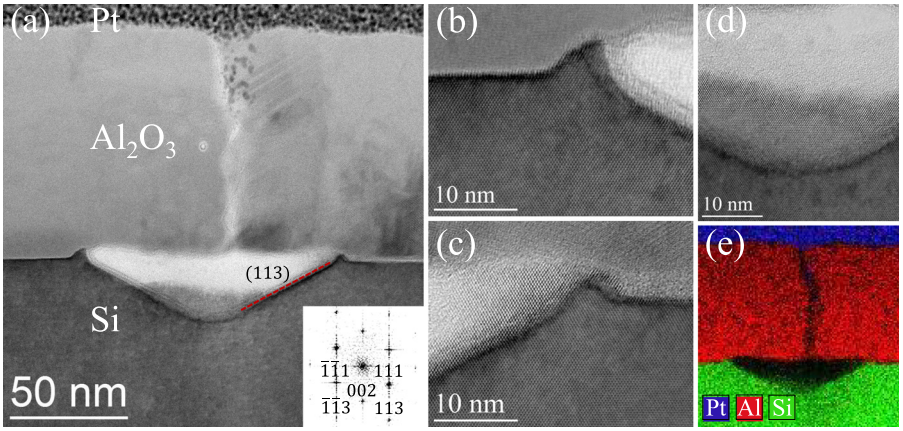

FIG. 2. Bright-field TEM images of the Al_2O_3 film. (a) An overview image of the blister site shows a cavity in Si with a crack extending from the cavity through the film. The inset shows the FFT image of the Si. (b)–(d) High-resolution images of the cavity area show no defects in Si {113} facets and that the accumulated Si at the edges is single-crystalline. (e) An EDX map of the blister site did not indicate interdiffusion between alumina and Si.

high biaxial compressive stress while the alumina film is in tensile stress based on the shift of the (012) α peak whose position is well defined in the literature. The biaxial stresses σ of the AlN and Al_2O_3 films were approximated based on $\sigma = \frac{E}{2\nu}\varepsilon$, where E is the Young's modulus, ν the Poisson's ratio, and ε the engineering strain of the corresponding lattice spacing calculated from the (002) and the (012) XRD peaks of AlN and Al_2O_3, respectively. For AlN, the constants were averaged from the data given in Ref. 24 for epi-quality AlN ($E = 324$ GPa, $\nu = 0.21$, and $d_{002} = 0.498$ nm), which gives an unrealistically high compressive stress of $\sigma = -14$ GPa most likely due to incorrect material constants. Likewise, the elastic constants for Al_2O_3 were taken from Ref. 25 using the constants given for grade "A4/A5" alumina and the lattice spacing of (012) from Ref. 23 ($E = 360$ GPa, $\nu = 0.25$, and $d_{012} = 0.697$ nm) giving a tensile stress of $\sigma = 3$ GPa likely also overestimating the true stress, as for a similar crystallized ALD alumina film, a tensile stress of 1 GPa is quoted in the literature.[26] A tensile stress could be expected for the as-deposited films too.[27] The calculations still highlight the very high compressive stress present in the AlN film and the high tensile stress in the Al_2O_3 film.

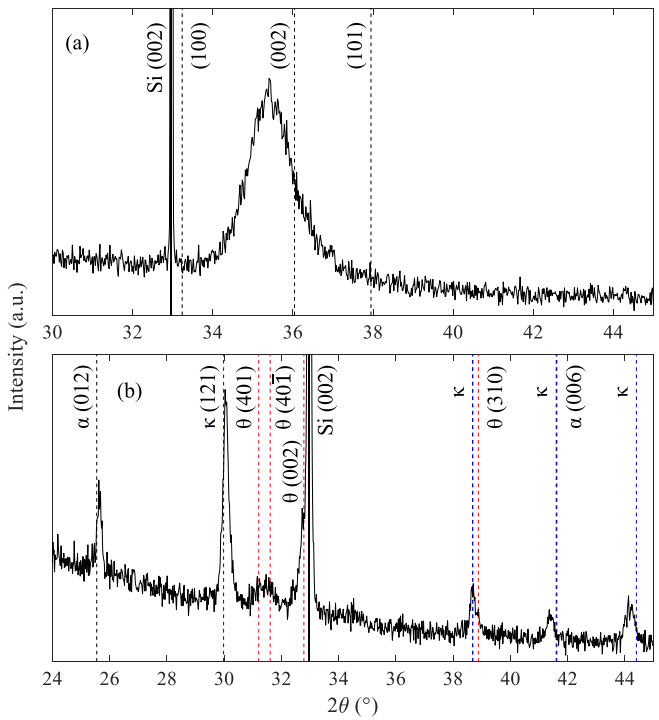

FIG. 3. XRD patterns of the AlN film (a) and the vacuum-annealed Al_2O_3 film (b). The XRD pattern of AlN indicates the film to be in a high compressive biaxial stress. The different phases in the Al_2O_3 graph (b) are marked with black (α), blue (κ), and red (θ). Peaks that are not indexed have several diffracting planes in close proximity. Black solid lines represent the ideal Si (002) reflections which coincide well with the measured peaks.

The ToF-ERD analyses are summarized in Table I, while Fig. 4 presents the depth profile of the annealed Al_2O_3 film (the other depth profiles are presented in Fig. S4, supplementary material). The AlN film can be considered high quality ALD AlN with little impurities compared to the literature.[13] Likewise, the Al_2O_3 is of high or similar quality compared to the literature.[28] The stoichiometry and carbon impurities did not change due to the annealing. Noteworthy is that the amount of hydrogen decreases to a one-third of the original concentration. Nevertheless, no hydrogen was concentrated at the Si interface after the annealing (Fig. 4).

Based on the results presented above, we propose that the blistering is driven by two different mechanisms in these ALD films. In the AlN film, the driving force comes from the high compressive biaxial stress, whereas in the Al_2O_3 film, the blistering mechanism is initiated by the cavitation of the substrate caused by the surface diffusion of Si atoms. The stress-driven mechanism has been extensively examined in physical vapor deposition (PVD) films.[29] Furthermore, the root cause behind the compressive stress of the PEALD AlN film is likely linked to the ion subplantation effect.[30] Some of the energetic particles reach the film causing collision cascades, leading to the densification of the film due to subplantation. The ToF-ERDA indeed revealed 0.06 at. % of Ar in the AlN film. The cavitation mechanism, on the other hand, is proposed to be similar to the one presented by Xie *et al.* [10] where hydrogen at the interface undermines the substrate-film bonds causing surface diffusion of the Si atoms. The hydrogen diffusion to the interface is driven by the heat

TABLE I. ToF-ERDA elemental compositions of the films. asd = as-deposited and hv = high vacuum.

Sample	Al (at. %)	O (at. %)	N (at. %)	H (at. %)	C (at. %)	Cl (at. %)
Al_2O_3 asd	39 ± 1	61 ± 2	…	0.21 ± 0.05	0.07 ± 0.03	…
Al_2O_3 hv	39 ± 1	61 ± 2	…	0.07 ± 0.03	0.08 ± 0.03	…
AlN	45 ± 2	1.7 ± 0.2	47 ± 2	6.5 ± 0.5	0.09 ± 0.03	0.1 ± 0.02

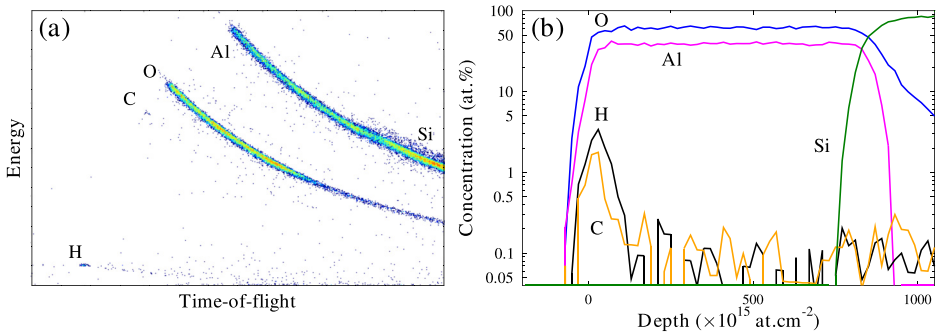

FIG. 4. (a) A raw ToF-energy histogram indicating the high quality of the measurement data and (b) the corresponding ToF-ERDA depth profile of the Al_2O_3 film annealed at 1000 °C in the high vacuum. The y axis in (b) is logarithmic.

treatment which also enhances the surface mobility of the Si atoms.[31] Compared to the literature,[2,8,9] blistering in ALD alumina films has been detected at much lower temperatures (annealing at 400 °C). However, in those studies, the deposition temperatures have been much lower, leading to a higher concentration of hydrogen[32] with different hydrogen trap state energies.[33] Nevertheless, the amount of hydrogen in the alumina film of this study should be enough to cover the Si (100) surface (calculation presented in the supplementary material). The cavity will reach a critical size, after which the internal gas pressure, together with the biaxial tensile stress, will be enough to deform the alumina film causing the observed crack in Fig. 2(a). The gaseous hydrogen will escape through these cracks which is why no additional hydrogen was detected at the silicon interface by ToF-ERDA. The blistering of alumina can be alleviated by choosing ALD parameters which produce a film with hydrogen at high energy trap states. Furthermore, the annealing atmosphere also plays a role in the crystallization behavior of ALD Al_2O_3[12] and hence in the detrapping of hydrogen. We propose that it is possible to crystallize ALD alumina without blistering by selecting an annealing temperature and atmosphere where the critical driving force, related to the hydrogen trap state energies, is not exceeded as demonstrated in Ref. 12.

See supplementary material for more images of the blisters, ToF-ERDA data, and a calculation of the total available hydrogen at the Si-Al_2O_3 interface.

This research was supported by the ECSEL2014-2-662155 project: Informed and Academy of Finland Center of Excellence in Nuclear and Accelerator Based Physics (Ref. 251353). The authors would like to thank Dr. Ulla Vainio for the help with the XRD. The research was conducted in the facilities of OtaNano, Aalto University; Fraunhofer IMWS, CAM; and the University of Jyväskylä. Al_2O_3 deposition was carried out at Beneq Oy. Wafers were provided by Okmetic Oy.

[1]S. Smith, W. M. Li, K. E. Elers, and K. Pfeifer, Microelectron. Eng. **64**, 247 (2002).
[2]O. Beldarrain, M. Duch, M. Zabala, J. M. Rafí, M. B. González, and F. Campabadal, J. Vac. Sci. Technol., A **31**, 01A128 (2013).
[3]K. Tapily, J. Jakes, P. Shrestha, and D. Gu, ECS Trans. **16**, 269 (2008).
[4]E. Beche, F. Fournel, V. Larrey, F. Rieutord, C. Morales, A.-M. Charvet, F. Madeira, G. Audoit, and J.-M. Fabbri, ECS J. Solid State Sci. Technol. **4**, P171 (2015).
[5]E. Marin, A. Lanzutti, M. Lekka, L. Guzman, W. Ensinger, and L. Fedrizzi, Surf. Coat. Technol. **211**, 84 (2012).
[6]B. Vermang, H. Goverde, A. Uruena, A. Lorenz, E. Cornagliotti, A. Rothschild, J. John, J. Poortmans, and R. Mertens, Sol. Energy Mater. Sol. Cells **101**, 204 (2012).
[7]T. Lüdera, T. Lauermann, A. Zuschlag, G. Hahn, and B. Terheiden, Energy Procedia **27**, 426 (2012).
[8]S. Li, P. Repo, G. Von Gastrow, Y. Bao, and H. Savin, in *Conference Record of the IEEE Photovoltaic Specialists Conference* (2013), p. 1265.
[9]B. Vermang, H. Goverde, V. Simons, I. D. Wolf, J. Meersschaut, S. Tanaka, J. John, J. Poortmans, and R. Mertens, in *38th IEEE Photovoltaic Specialists Conference (PVSC)* (2012), pp. 1135–1138.
[10]D.-G. Xie, Z.-J. Wang, J. Sun, J. Li, E. Ma, and Z.-W. Shan, Nat. Mater. **14**, 899 (2015).
[11]L. Hennen, E. H. A. Granneman, and W. M. M. Kessels, in *38th IEEE Photovoltaic Specialists Conference (PVSC), 2012* (2011), p. 1049.
[12]M. Broas, O. Kanninen, V. Vuorinen, M. Tilli, and M. Paulasto-Kröckel, ACS Omega **2**, 3390 (2017).
[13]M. Broas, P. Sippola, T. Sajavaara, V. Vuorinen, A. Pyymaki Perros, H. Lipsanen, and M. Paulasto-Kröckel, J. Vac. Sci. Technol., A **34**, 41506 (2016).
[14]M. Laitinen, M. Rossi, J. Julin, and T. Sajavaara, Nucl. Instrum. Methods Phys. Res., Sect. B **337**, 55 (2014).
[15]S. D. Elliott, G. Scarel, C. Wiemer, M. Fanciulli, and G. Pavia, Chem. Mater. **18**, 3764 (2006).
[16]H. Van Bui, M. D. Nguyen, F. B. Wiggers, A. A. I. Aarnink, M. P. de Jong, and A. Y. Kovalgin, ECS J. Solid State Sci. Technol. **3**, P101 (2014).
[17]Y. J. Lee and S.-W. Kang, Thin Solid Films **446**, 227 (2004).
[18]J. M. Gibson, M. L. McDonald, and F. C. Unterwald, Phys. Rev. Lett **55**, 1765 (1985).
[19]S. Hong, J. Korean Phys. Soc. **37**, 93 (2000).
[20]H. Schulz and K. H. Thiemann, Solid State Commun. **23**, 815 (1977).
[21]B. Ollivier, R. Retoux, P. Lacorre, D. Massiot, and G. Férey, J. Mater. Chem. **7**, 1049 (1997).
[22]E. Husson and Y. Repelin, Eur. J. Solid State Inorg. Chem. **33**, 1223 (1996).
[23]D. E. Cox, A. R. Moodenbaugh, A. W. Sleight, and H. Y. Chen, in *Proceedings of Symposium on Accuracy in Powder Diffraction, National Bureau of Standards, Gaithersburg, MD, 11–15 June, 1979* (1980), p. 189.
[24]M. A. Moram and M. E. Vickers, Rep. Prog. Phys. **72**, 36502 (2009).
[25]P. Auerkari, Tech. Res. Cent. Finl. **1792**, 26 (1996).
[26]R. L. Puurunen, J. Saarilahti, and H. Kattelus, ECS Trans. **11**, 3 (2007).
[27]O. M. E. Ylivaara, X. Liu, L. Kilpi, J. Lyytinen, D. Schneider, M. Laitinen, J. Julin, S. Ali, S. Sintonen, M. Berdova, E. Haimi, T. Sajavaara, H. Ronkainen, H. Lipsanen, J. Koskinen, S. P. Hannula, and R. L. Puurunen, Thin Solid Films **552**, 124 (2014).
[28]R. Matero, A. Rahtu, M. Ritala, M. Leskelä, and T. Sajavaara, Thin Solid Films **368**, 1 (2000).
[29]L. Ben Freund and S. Suresh, *Thin Film Materials: Stress, Defect Formation and Surface Evolution* (Cambridge University Press, 2004).
[30]H. B. Profijt, M. C. M. van de Sanden, and W. M. M. Kessels, J. Vac. Sci. Technol., A **31**, 01A106 (2013).
[31]P. E. Acosta-Alba, O. Kononchuk, C. Gourdel, and A. Claverie, J. Appl. Phys. **115**, 134903 (2014).
[32]M. D. Groner, F. H. Fabreguette, J. W. Elam, and S. M. George, Chem. Mater. **16**, 639 (2004).
[33]G. A. Young and J. R. Scully, Acta Mater. **46**, 6337 (1998).